Article

Glutathione-Protected Gold Clusters Revisited: Bridging the Gap between Gold(I)–Thiolate Complexes and Thiolate-Protected Gold Nanocrystals

Yuichi Negishi, Katsuyuki Nobusada, and Tatsuya Tsukuda

J. Am. Chem. Soc., **2005**, 127 (14), 5261-5270• DOI: 10.1021/ja042218h • Publication Date (Web): 18 March 2005

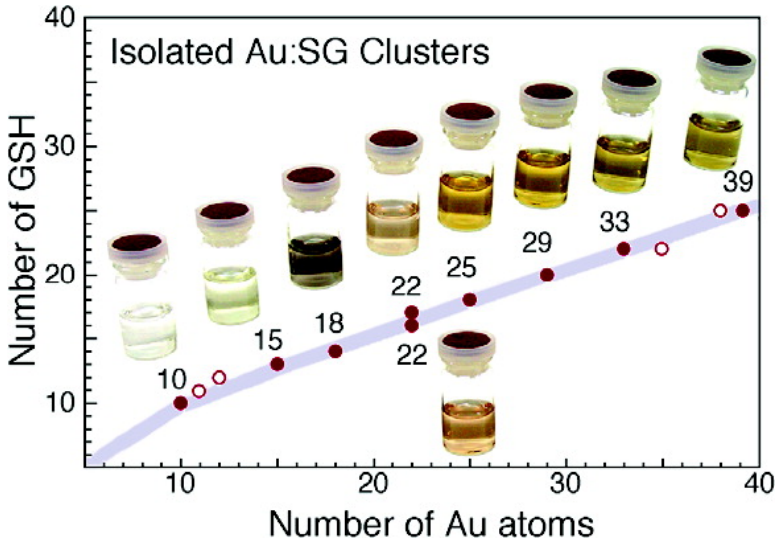

More About This Article

Additional resources and features associated with this article are available within the HTML version:

- Supporting Information
- Links to the 43 articles that cite this article, as of the time of this article download
- Access to high resolution figures
- Links to articles and content related to this article
- Copyright permission to reproduce figures and/or text from this article

View the Full Text HTML

J|A|C|S
ARTICLES
Published on Web 03/18/2005

Glutathione-Protected Gold Clusters Revisited: Bridging the Gap between Gold(I)−Thiolate Complexes and Thiolate-Protected Gold Nanocrystals

Yuichi Negishi,[†,‡] Katsuyuki Nobusada,[§] and Tatsuya Tsukuda*[,†,‡]

Contribution from the Research Center for Molecular-Scale Nanoscience and Department of Theoretical Studies, Institute for Molecular Science, Myodaiji, Okazaki 444-8585, Japan, and Department of Photoscience, School of Advanced Sciences, The Graduate University for Advanced Studies, Hayama, Kanagawa 240-0193, Japan

Received December 27, 2004; E-mail: tsukuda@ims.ac.jp

Abstract: Small gold clusters (~1 nm) protected by molecules of a tripeptide, glutathione (GSH), were prepared by reductive decomposition of Au(I)−SG polymers at a low temperature and separated into a number of fractions by polyacrylamide gel electrophoresis (PAGE). Chemical compositions of the fractionated clusters determined previously by electrospray ionization (ESI) mass spectrometry (Negishi, Y. et al. *J. Am. Chem. Soc.* **2004**, *126*, 6518) were reassessed by taking advantage of freshly prepared samples, higher mass resolution, and more accurate mass calibration; the nine smallest components are reassigned to $Au_{10}(SG)_{10}$, $Au_{15}(SG)_{13}$, $Au_{18}(SG)_{14}$, $Au_{22}(SG)_{16}$, $Au_{22}(SG)_{17}$, $Au_{25}(SG)_{18}$, $Au_{29}(SG)_{20}$, $Au_{33}(SG)_{22}$, and $Au_{39}(SG)_{24}$. These assignments were further confirmed by measuring the mass spectra of the isolated Au:S(h-G) clusters, where h-GSH is a homoglutathione. It is proposed that a series of the isolated Au:SG clusters corresponds to kinetically trapped intermediates of the growing Au cores. The relative abundance of the isolated clusters was correlated well with the thermodynamic stabilities against unimolecular decomposition. The electronic structures of the isolated Au:SG clusters were probed by X-ray photoelectron spectroscopy (XPS) and optical spectroscopy. The Au(4f) XPS spectra illustrate substantial electron donation from the gold cores to the GS ligands in the Au:SG clusters. The optical absorption and photoluminescence spectra indicate that the electronic structures of the Au:SG clusters are well quantized; embryos of the sp band of the bulk gold evolve remarkably depending on the number of the gold atoms and GS ligands. The comparison of these spectral data with those of sodium Au(I) thiomalate and 1.8 nm Au:SG nanocrystals (NCs) reveals that the subnanometer-sized Au clusters thiolated constitute a distinct class of binary system which lies between the Au(I)−thiolate complexes and thiolate-protected Au NCs.

1. Introduction

Interaction between gold and thiols has attained considerable importance in wide areas of modern science from both fundamental and practical viewpoints. The main reason for such a situation is that a variety of useful compounds, materials, functionalized thin films, and nanofabricated structures are provided through the chemical bonding between gold and thiols (most likely in the form of thiolates). The Au−thiolate binary systems exhibit unique structures and properties depending on degree of aggregation of the Au atoms and are categorized into the following groups (Scheme 1): Au(I)−thiolate complexes; Au nanocrystals (NCs) protected by thiolate monolayers; self-assembled monolayers (SAMs) on extended Au surfaces.

Au(I)−thiolate complexes correspond to the smallest binary system. Some of the Au(I)−thiolate complexes (e.g., Myochrisine, Solganol) have widely been used as therapeutic agents for the treatment of rheumatoid arthritis over the half-century.[1,2] The binding of Au(I) to metallothioneins, cysteine-containing proteins, has also been studied to understand their physiological functions.[3] The extended X-ray absorption fine structure (EXAFS), wide-angle X-ray scattering (WAXS), and X-ray diffraction (XRD) studies have revealed that most of the Au(I)−thiolate complexes exhibit gold-to-thiolate ratios close to 1:1 and tend to form polymeric structures with −Au−S(R)− repeated bondings.[1,4−6] Another important factor that affects the structures and photophysical properties of the Au(I)−thiolate complexes[7−11] is that Au(I) atoms with a d^{10} closed-shell

[†] Research Center for Molecular-Scale Nanoscience, Institute for Molecular Science.
[‡] The Graduate University for Advanced Studies.
[§] Department of Theoretical Studies, Institute for Molecular Science.

(1) Shaw, C. F. *Chem. Rev.* **1999**, *99*, 2589.
(2) Corey, E. J.; Mehrotra, M. M.; Khan, A. U. *Science* **1987**, *236*, 68.
(3) Schmitz, G.; Minkel, D. T.; Gingrich, D.; Shaw, C. F., III. *J. Inorg. Biochem.* **1980**, *12*, 293.
(4) LeBlanc, D. J.; Smith, R. W.; Wang, Z.; Howard-Lock, H. E.; Lock, C. J. L. *J. Chem. Soc., Dalton Trans.* **1997**, 3263.
(5) Bau, R. *J. Am. Chem. Soc.* **1998**, *120*, 9380.
(6) Bachman, R. E.; Bodolosky-Bettis, S. A.; Glennon, S. C.; Sirchio, S. A. *J. Am. Chem. Soc.* **2000**, *122*, 7146.
(7) Jones, W. B.; Yuan, J.; Narayanaswany, R.; Young, M. A.; Elder, R. C.; Bruce, A. E.; Bruce, M. R. M. *Inorg. Chem.* **1995**, *34*, 1996.
(8) Forward, J. M.; Bohmann, D.; Fackler, J. P., Jr.; Staples, R. J. *Inorg. Chem.* **1995**, *34*, 6330.
(9) Kunkely, H.; Vogler, A. *Z. Naturforsch.* **1996**, *51b*, 1067.
(10) Yam, V. W.-W.; Li, C.-K.; Chan, C.-L. *Angew. Chem., Int. Ed.* **1998**, *37*, 2857.

Scheme 1. Evolution of Gold−Thiolate Binary Systems as a Function of the Number of Gold Atoms

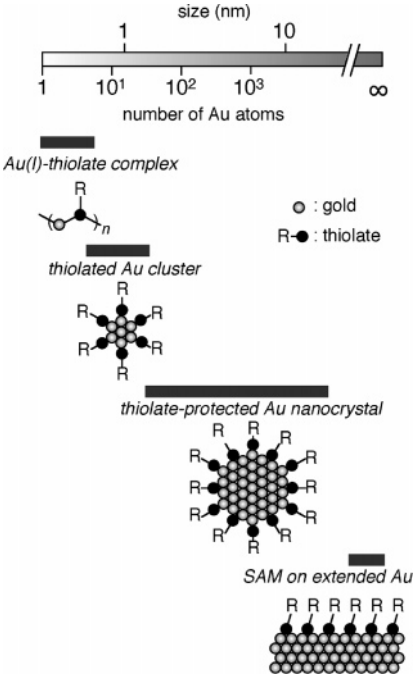

electronic configuration tend to form aggregates through so-called "aurophilic" interaction.[12] The relatively strong noncovalent Au(I)−Au(I) interaction is attributed to hybridization between the empty 6s/6p shells and filled $5d^{10}$ shells which are stabilized and destabilized, respectively, due to the relativistic effect. On the other hand, the binary system which locates at the opposite limit is a well-ordered and densely packed thiolate monolayer film on an extended Au surface, well-known as a self-assembled monolayer (SAM).[13] The SAMs have aroused huge interest because of the great potentiality in applications for chemical sensing, corrosion inhibition, lubrication, catalysis, biosensing, biomimetics, and biocompatibility. The spontaneous bond formation between thiolates and Au surfaces also provides a basis for the fabrication of a molecular junction for electronic devices[14] and nanoscale patterning via microcontact printing[15] and dip-pen nanolithography.[16] The number ratios between thiolates and surface Au atoms are dependent on both the structures of the thiolates and the surfaces; the ratio is 1:3 for the *n*-alkanethiolate SAMs with the $(\sqrt{3} \times \sqrt{3})$ *R*30° superlattice structure formed on Au(111). Regardless of the extensive studies on the SAM structures, the exact location of the sulfur headgroup on the Au surface is still in debate.[17]

The simple chemical preparation exploited by Schiffrin and co-workers[18] has opened up a third class of gold−thiolate binary systems that lies between the two limiting systems described above.[19−22] The preparation is based on the chemical reduction of Au ions in the presence of thiols (or reductive decomposition of Au(I)−thiolate polymers) and yields Au(0) nanocrystals (NCs) protected by the thiolate monolayers.[23] The thiolate-protected Au NCs offer a novel opportunity to study size-dependent evolution of the structures and fundamental properties of the Au NCs. To these ends, various methods have been developed so far to prepare sufficiently monodisperse Au NCs of any desired size by optimizing the preparation conditions (e.g., gold-to-thiol ratio, solvent temperature, reducing agent),[24,25] fractional precipitation,[26−28] size-exclusion chromatography (SEC),[29,30] heat treatment,[31] or chemical etching.[32] Through these efforts, it is now established that the optical properties,[25,27,28,32,33] geometrical structures,[34,35] and quantized charging behaviors[36−39] of the thiolate-protected Au NCs are well represented by the diameters of the seemingly spherical cores observed by transmission electron microscopy (TEM) or the number of the core atoms determined by mass spectrometry. The passivation by the thiolates has little influence on the properties of the underlying Au NCs, although the structure and dynamic behavior of the thiolate monolayer are modified to some extent from those of the corresponding two-dimensional SAM due to larger curvature of the NC surface.[40−43] With a basic knowledge of core-size dependent properties, an increasing number of researchers have been using the thiolate-protected Au NCs as elementary units

(11) Mansour, M. A.; Connick, W. B.; Lachicotte, R. J.; Gysling, H. J.; Eisenberg, R. *J. Am. Chem. Soc.* **1998**, *120*, 1329.
(12) See, for example: Pyykkö, P. *Angew. Chem., Int. Ed.* **2004**, *43*, 4412 and references therein.
(13) See, for example: Ulman, A. *Chem. Rev.* **1996**, *96*, 1533 and references therein.
(14) Reed, M. A.; Zhou, C.; Muller, C. J.; Burgin, T. P.; Tour, J. M. *Science* **1997**, *278*, 252.
(15) Wilbur, J. L.; Kumar, A.; Kim, E.; Whitesides, G. M. *Adv. Mater.* **1994**, *6*, 600.
(16) Piner, R. D.; Zhu, J.; Xu, F.; Hong, S.; Mirkin, C. A. *Science* **1999**, *283*, 661.
(17) See, for example: Kondoh, H.; Iwasaki, M.; Shimada, T.; Amemiya, K.; Yokoyama, T.; Ohta, T.; Shimomura, M.; Kono, S. *Phys. Rev. Lett.* **2003**, *90*, 066102.
(18) Brust, M.; Walker, M.; Bethell, D.; Schiffrin, D. J.; Whyman, R. *J. Chem. Soc., Chem. Commun.* **1994**, 801.
(19) Whetten, R. L.; Khoury, J. T.; Alvarez, M. M.; Murthy, S.; Vezmar, I.; Wang, Z. L.; Stephens, P. W.; Cleveland, C. L.; Luedtke, W. D.; Landman, U. *Adv. Mater.* **1996**, *8*, 428.
(20) Whetten, R. L.; Shafigullin, M. N.; Khoury, J. T.; Schaaff, T. G.; Vezmar, I.; Alvarez, M. M.; Wilkinson, A. *Acc. Chem. Res.* **1999**, *32*, 397.
(21) Templeton, A. C.; Wuelfing, W. P.; Murray, R. W. *Acc. Chem. Res.* **2000**, *33*, 27.
(22) Daniel, M.-C.; Astruc, D. *Chem. Rev.* **2004**, *104*, 293 and references therein.
(23) These systems are often referred to as monolayer-protected clusters (MPCs) in a broad sense (ref 21). We call the particles smaller and larger than ~1.5 nm as "cluster" and "nanocrystals", respectively.
(24) Leff, D. V.; Ohara, P. C.; Heath, J. R.; Gelbart, W. M. *J. Phys. Chem.* **1995**, *99*, 7036.
(25) Hostetler, M. J.; Wingate, J. E.; Zhong, C.-J.; Harris, J. E.; Vachet, R. W.; Clark, M. R.; Londono, J. D.; Green, S. J.; Stokes, J. J.; Wignall, G. D.; Glish, G. L.; Porter, M. D.; Evans, N. D.; Murray, R. W. *Langmuir* **1998**, *14*, 17.
(26) Alvarez, M. M.; Khoury, J. T.; Schaaff, T. G.; Shafigullin, M.; Vezmar, I.; Whetten, R. L. *Chem. Phys. Lett.* **1997**, *266*, 91.
(27) Alvarez, M. M.; Khoury, J. T.; Schaaff, T. G.; Shafigullin, M. N.; Vezmar, I.; Whetten, R. L. *J. Phys. Chem. B* **1997**, *101*, 3706.
(28) Schaaff, T. G.; Shafigullin, M. N.; Khoury, J. T.; Vezmar, I.; Whetten, R. L.; Cullen, W. G.; First, P. N.; Gutiérrez-Wing, C.; Ascensio, J.; Jose-Yacamán, M. J. *J. Phys. Chem. B* **1997**, *101*, 7885.
(29) Wilcoxon, J. P.; Martin, J. E.; Provencio, P. *Langmuir* **2000**, *16*, 9912.
(30) Murayama, H.; Narushima, T.; Negishi, Y.; Tsukuda, T. *J. Phys. Chem. B* **2004**, *108*, 3496.
(31) Shimizu, T.; Teranishi, T.; Hasegawa, S.; Miyake, M. *J. Phys. Chem. B* **2003**, *107*, 2719.
(32) Schaaff, T. G.; Whetten, R. L. *J. Phys. Chem. B* **1999**, *103*, 9394.
(33) Schaaff, T. G.; Shafigullin, M. N.; Khoury, J. T.; Vezmar, I.; Whetten, R. L. *J. Phys. Chem. B* **2001**, *105*, 8785.
(34) Cleveland, C. L.; Landman, U.; Schaaff, T. G.; Shafigullin, M. N.; Stephens, P. W.; Whetten, R. L. *Phys. Rev. Lett.* **1997**, *79*, 1873.
(35) Zanchet, D.; Hall, B. D.; Ugarte, D. *J. Phys. Chem. B* **2000**, *104*, 11013.
(36) Ingram, R. S.; Hostetler, M. J.; Murray, R. W.; Schaaff, T. G.; Khoury, J. T.; Whetten, R. L.; Bigioni, T. P.; Guthrie, D. K.; First, P. N. *J. Am. Chem. Soc.* **1997**, *119*, 9279.
(37) Chen, S.; Ingram, R. S.; Hostetler, M. J.; Pietron, J. J.; Murray, R. W.; Schaaff, T. G.; Khoury, J. T.; Alvarez, M. M.; Whetten, R. L. *Science* **1998**, *280*, 2098.
(38) Bigioni, T. P.; Harrell, L. E.; Cullen, W. G.; Guthrie, D. K.; Whetten, R. L.; First, P. N. *Eur. Phys. J. D* **1999**, *6*, 355.
(39) Quinn, B. M.; Liljeroth, P.; Ruiz, V.; Laaksonen, T.; Kontturi, K. *J. Am. Chem. Soc.* **2003**, *125*, 6644.
(40) Luedtke, W. D.; Landman, U. *J. Phys. Chem.* **1996**, *100*, 13323.
(41) Luedtke, W. D.; Landman, U. *J. Phys. Chem. B* **1998**, *102*, 6566.
(42) Hostetler, M. J.; Stokes, J. J.; Murray, R. W. *Langmuir* **1996**, *12*, 3604.
(43) Badia, A.; Cuccia, L.; Demers, L.; Morin, F.; Lennox, R. B. *J. Am. Chem. Soc.* **1997**, *119*, 2682.

in fabricating highly ordered superstructures, nanodevices, and sensors.[22]

When the dimension of the Au core is reduced below 1.5 nm, the population of the Au atoms located at the core−ligand interface increases markedly. As a result, one can anticipate that the thiolate ligation starts to play a significant role in determining the structures and properties of the binary system. Indeed, theoretical studies have shown that the thiolate ligation against such small clusters exerts direct influence on their geometric and electronic structures, such as charge transfer at the Au−S interface[44,45] and deformation of the core structures.[46−49] Because of these remarkable surface effects together with the core size effect, small Au clusters protected by thiolates exhibit novel properties that are totally absent in the bulk gold. Recent examples include photoluminescence,[50−57] ferromagnetism,[58] optical chirality,[47,48,59] and redox-type charging behavior.[37,56,60] Thus, these small binary systems are best represented in terms of the chemical compositions (i.e., the number of the constituent Au atoms and the thiolates) and should be discriminated from the thiolate-protected Au NCs characterized mostly by the core dimensions. In this context, we designate these small systems as "thiolated Au clusters" in the present paper (Scheme 1). A number of methods have been reported so far for the preparation of the thiolated Au clusters with nearly single compositions.[54−57,61−65] However, the origin of their novel properties has not yet been understood partly due to the difficulties in synthesizing the clusters with well-defined compositions in a systematic manner. Since the preparation methods are based on nucleation of Au cores in the presence of thiols, the sizes of the resulting clusters are inevitably distributed due to statistical fluctuations in the nucleation process. Thus, an indispensable task to obtain well-defined clusters is to develop a high-resolution fractionation method of the as-prepared thiolated clusters and mass spectroscopic characterization of the fractionated clusters. Recently, Whetten and co-workers have succeeded in fractionation of Au clusters protected by monolayers of glutathione (GSH; see Scheme 2) by using polyacrylamide gel electrophoresis (PAGE) and identified the most abundant species as $Au_{28}(SG)_{16}$ by mass spectrometry.[59,61] In the previous paper, we have reported chemical compositions of a wider range of PAGE-separated Au:SG clusters by extensive mass spectrometric measurement.[57] The present paper describes a full account of selective synthesis and characterization of the Au:SG clusters. Main objectives of the present study include the following: (i) establishment of a versatile and reproducible experimental method to synthesize a series of thiolated Au clusters with well-defined compositions; (ii) clarification of correlation of structures and stabilities with the chemical compositions of the thiolated Au clusters. The results reported here will contribute to the basic understanding of how the structures of the Au−thiolate binary systems evolve going from the Au(I)−thiolate complexes to thiolate-protected Au NCs and will provide a useful guideline for the development of novel organometallic clusters.

Scheme 2. Molecular Structures of Glutathione (GSH) and Homoglutathione (h-GSH)

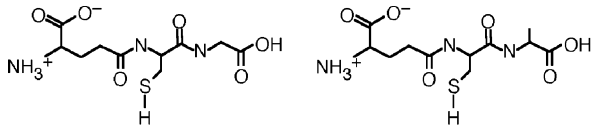

2. Experimental Section

2.1. Chemicals. All of the chemicals were commercially available and used without further purification. Sodium Au(I) thiomalate (SGT) was supplied from Shionogi Co. Ltd. Hydrogen tetrachloroaurate tetrahydrate, sodium tetrahydroborate, and glutathione in the reduced form (GSH, $M_w = 307$) were obtained from Wako Pure Chemical Industries. Homoglutathione (h-GSH, $M_w = 321$) was purchased from Bachem. The molecular structures of GSH and h-GSH are shown in Scheme 2. The deionized water with the resistivity of >18 MΩ cm was used in the present study.

2.2. Preparation of Au:SG and Au:S(h-G) Clusters. The preparation method employed here is similar to those reported previously.[57,59,61,66] To the methanol solution (50 mL) of $HAuCl_4$ (0.25 mmol) was added 1.0 mmol of GSH or h-GSH. The mixture was then cooled to ∼0 °C in a cool bath for 30 min. Then, the aqueous solution of $NaBH_4$ (0.2 M, 12.5 mL), cooled at ∼0 °C, was injected rapidly into this mixture under vigorous stirring. The mixture was allowed to react for another hour. The resulting precipitate was collected and washed repeatedly with methanol through centrifugal precipitation or by centrifugal ultrafiltration to remove the remaining starting materials. Finally, the precipitate was dried in vacuo to obtain the Au:SG or Au:S(h-G) clusters as a dark-brown powder.

2.3. Polyacrylamide Gel Electrophoresis (PAGE).[57,59,61] PAGE experiment was carried out by using a slab gel electrophoresis unit, which employs a single (NA1120, NIHON EIDO) or six (NA1116P, NIHON EIDO) gel(s) with a size of 3t × 160 × 160 mm. A typical procedure for the separation with a single gel will be described below. The separating and stacking gels were prepared by acrylamide monomers with the total contents of 30 and 3 wt % (acrylamide/bis(acrylamide) = 94:6), respectively. The eluting buffer consisted of 192 mM glycine and 25 mM tris(hydroxymethylamine). The as-prepared Au:SG clusters were dissolved in a 5% (v/v) glycerol/water solution (0.5 mL) at a concentration of 60 mg/mL. The sample solution (0.5 mL) was loaded onto the stacking gel without lanes and eluted for 9 h at a constant voltage mode (150 V) to achieve sufficient separation.

(44) Häkkinen, H.; Barnett, R. N.; Landman, U. *Phys. Rev. Lett.* **1999**, *82*, 3264.
(45) Larsson, J. A.; Nolan, M.; Greer, J. C. *J. Phys. Chem. B* **2002**, *106*, 5931.
(46) Garzón, I. L.; Rovira, C.; Michaelian, K.; Beltrán, M. R.; Ordejón, P.; Junquera, J.; Sánchez-Portal, D.; Artacho, E.; Soler, J. M. *Phys. Rev. Lett.* **2000**, *85*, 5250.
(47) Garzón, I. L.; Reyes-Nava, J. A.; Rodríguez-Hernández, J. I.; Sigal, I.; Beltrán, M. R.; Michaelian, K. *Phys. Rev. B* **2002**, *66*, 073403.
(48) Román-Velázquez, C. E.; Noguez, C.; Garzón, I. L. *J. Phys. Chem. B* **2003**, *107*, 12035.
(49) Wilson, N. T.; Johnston, R. L. *Phys. Chem. Chem. Phys.* **2002**, *4*, 4168.
(50) Bigioni, T. P.; Whetten, R. L.; Dag, Ö. *J. Phys. Chem. B* **2000**, *104*, 6983.
(51) Huang, T.; Murray, R. W. *J. Phys. Chem. B* **2001**, *105*, 12498.
(52) Link, S.; Beeby, A.; Fitzgerald, S.; El-Sayed, M. A.; Schaaff, T. G.; Whetten, R. L. *J. Phys. Chem. B* **2002**, *106*, 3410.
(53) Link, S.; El-Sayed, M. A.; Schaaff, T. G.; Whetten, R. L. *Chem. Phys. Lett.* **2002**, *356*, 240.
(54) Yang, Y.; Chen, S. *Nano Lett.* **2003**, *3*, 75.
(55) Negishi, Y.; Tsukuda, T. *Chem. Phys. Lett.* **2004**, *383*, 161.
(56) Lee, D.; Donkers, R. L.; Wang, G.; Harper, A. S.; Murray, R. W. *J. Am. Chem. Soc.* **2004**, *126*, 6193.
(57) Negishi, Y.; Takasugi, Y.; Sato, S.; Yao, H.; Kimura, K.; Tsukuda T. *J. Am. Chem. Soc.* **2004**, *126*, 6518.
(58) Crespo, P.; Litrán, R.; Rojas, T. C.; Multigner, M.; de la Fuente, J. M.; Sánchez-López, J. C.; García, M. A.; Hernando, A.; Penadés, S.; Fernández, A. *Phys. Rev. Lett.* **2004**, *93*, 087204.
(59) Schaaff, T. G.; Whetten, R. L. *J. Phys. Chem. B* **2000**, *104*, 2630.
(60) Lee, D.; Donkers, R. L.; DeSimone, J. M.; Murray, R. W. *J. Am. Chem. Soc.* **2003**, *125*, 1182.
(61) Schaaff, T. G.; Knight, G.; Shafigullin, M. N.; Borkman, R. F.; Whetten, R. L. *J. Phys. Chem. B* **1998**, *102*, 10643.
(62) Woehrle, G. H.; Warner, M. G.; Hutchison, J. E. *J. Phys. Chem. B* **2002**, *106*, 9979.
(63) Negishi, Y.; Tsukuda, T. *J. Am. Chem. Soc.* **2003**, *125*, 4046.
(64) Donkers, R. L.; Lee, D.; Murray, R. W. *Langmuir* **2004**, *20*, 1945.
(65) Jin, R.; Egusa, S.; Scherer, N. F. *J. Am. Chem. Soc.* **2004**, *126*, 9900.
(66) Chen, S.; Yao, H.; Kimura, K. *Langmuir* **2001**, *17*, 733.

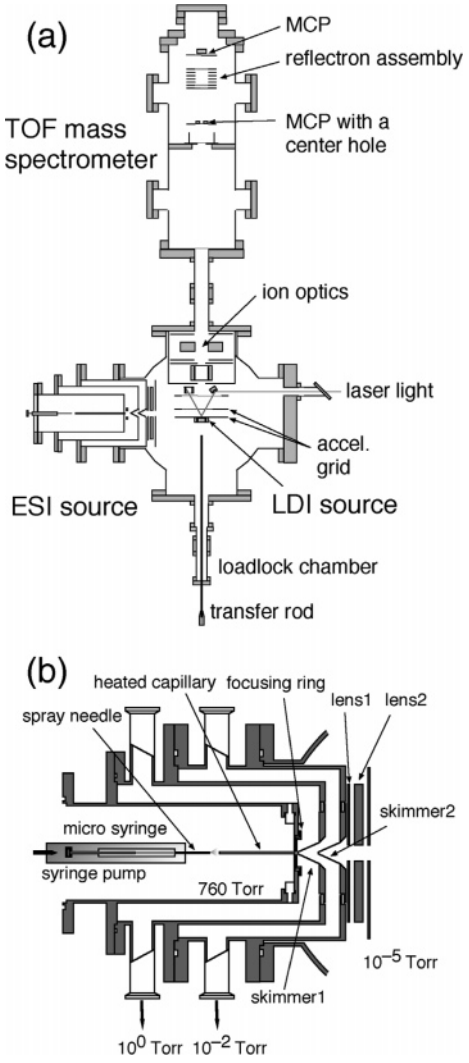

Figure 1. (a) Schematic view of the TOF mass spectrometer equipped with electrospray ionization (ESI) and laser desorption ionization (LDI) sources, and (b) the details of the ESI source.

To minimize the possibility of thermal decomposition of the clusters, the elution was performed in a refrigerator. Parts of the separating gel containing the fractions were cut out, crushed, and placed in distilled water (2 mL) for 2 h at 2 °C. The gel lumps suspended in the solution were removed by using a filter with 0.2 μm pores. After the addition of 2% acetic acid (1 mL), the sample solutions were concentrated to ~200 μL. The Au:SG clusters were precipitated by addition of methanol (1.5 mL) and subsequent centrifugation (14 000*g*). Then, the precipitate was redissolved in water (600 μL) and washed by centrifugal ultrafiltration (14 000*g*) twice to remove small impurities; a filter with a cutoff molecular weight of 5 kDa was used.

2.4. Electrospray Ionization (ESI) Mass Spectrometry.[57,59,61] ESI mass spectra of the fractionated samples were measured by using a homemade apparatus.[57] Figure 1a is a schematic representation of the top view of the whole experimental apparatus, which consists of the five stages of differentially pumped vacuum chambers. The apparatus accommodates an ESI source for production of gaseous ions of metal clusters dispersed in solvent[57] and a time-of-flight (TOF) mass spectrometer with a reflectron, which was newly introduced in the present study; a laser-desorption ionization (LDI) source[55,63] was not used in the present study. The details of the ESI source are depicted in Figure 1b, together with typical pressures of the chambers under operation. The 50% (v/v) water/methanol solutions of the Au:SG clusters with a concentration of 0.5 mg/mL were electrosprayed into the ambient atmosphere through a stainless steel needle of a syringe biased at ca. −3 kV. The solution was delivered by a syringe pump (SP310I, World Precision Instrument) at a typical flow rate of 2 μL/min; the syringe pump was mounted on an *xyz* stage to optimize the needle position. The central part of the sprayed cone containing large droplets was fed into a capillary heated resistively to promote desolvation. Under an optimized capillary temperature (ca. 180 °C), evaporation of the solvents from the droplets proceeds efficiently so that only the desolvated cluster ions in the intact form were formed at maximum yield. We observed dissociation of the intact clusters into small fragments, such as $[Au(SG)_2\text{-}H]^{-1}$ and $[Au_2(SG)_2\text{-}H]^{-1}$, at higher capillary temperatures. The cluster ions exiting the capillary were focused by a ring electrode, skimmed by two sets of skimmers, and guided by einzel lens toward an acceleration region of the TOF mass spectrometer of a Wiley−McLaren-type configuration. The ions were extracted perpendicularly to the initial beam by applying a pulsed high voltage (ca. −9 to −14 kV with ~30 ns rise time and 100 μs duration) to the acceleration grids. After stirred and focused by sets of ion optics, the ions were counted either by a microchannel plate detector located at the end of the flight path (F4655-10, Hamamatsu) or by that with a center hole (LPD-25, Burle) after reflected back by a retarding field of the reflectron. The repetition rate was 130 Hz, and spectra presented in this paper were obtained by accumulation for 5−40 min. Resolutions of the mass spectrometer ($M/\Delta M$) with and without the reflectron were typically 1000 and 400, respectively. The ESI mass spectra obtained were calibrated by referencing with that of $Na_nI_{n+1}^-$ cluster anions recorded under the same conditions.

2.5. Transmission Electron Microscope (TEM). It is important to disassemble the Au:SG clusters to evaluate their individual core diameters by means of TEM since they tend to form aggregates through hydrogen bonding between the COOH groups.[55,57,63,67,68] To this end, the pH value of the aqueous solution was set to 7.2, higher than the pK_a values of GSH (2.56 and 3.50),[69] so that the Au:SG clusters were repelled by each other due to the Coulomb repulsion between the COO^- groups of the GS ligands. The disassembled clusters were subsequently extracted into toluene phase via ion-pair formation with the tetraoctylammonium ions so that the cluster surfaces were modified into hydrophobic layers.[55,57,63,70] TEM specimens were prepared by drop-casting one or two drops of the toluene solutions onto a carbon-coated collodion film supported on a copper grid. Bright field TEM images were acquired with an electron microscope operated at 100 kV (H-7500, HITACHI). Typical magnification of the images was 100 000.

2.6. Optical Absorption and Photoluminescence (PL) Spectroscopy. UV−vis absorption and PL spectra of the Au:SG clusters were recorded in aqueous solutions at ambient temperature by using a double-beam spectrophotometer (U-2010, HITACHI) and a spectrofluorometer (FP-6600, JASCO), respectively. The sample solutions were not deaerated prior to the measurement. The cluster concentrations for the PL measurement were typically <10 μM, where the PL intensities increase linearly with the cluster concentrations. The emission and excitation spectra presented in the present paper correspond to the cross sections across the peak of three-dimensional PL spectra; the 3D PL spectra were composed of the bundles of the emission spectra obtained by scanning the excitation wavelengths in the range of 300−900 nm. The PL quantum yield, Φ_{PL}, was determined by comparison with the known yield (0.4%) of emission at 700 nm from a laser dye, LDS 750. The spectrofluorometer was calibrated by a standard lamp unit (ESC-333, JASCO) so that the PL profiles reported here are significantly modified with those reported previously.[57] The raw spectral data, $I(w)$, which are functions of wavelength, were converted to the energy-dependent data, $I(E)$, according to the following relation so that the

(67) Simard, J.; Briggs, C.; Boal, A. K.; Rotello, V. M. *Chem. Commun.* **2000**, 1943.
(68) Shiraishi, Y.; Arakawa, D.; Toshima, N. *Eur. Phys. J. E* **2002**, *8*, 377.
(69) Takehara, K.; Ide, Y.; Aihara, M.; Obuchi, E. *Bioelectrochem. Bioenerg.* **1992**, *29*, 103.
(70) Yao, H.; Momozawa, O.; Hamatani, T.; Kimura, K. *Bull. Chem. Soc. Jpn.* **2000**, *73*, 2675.

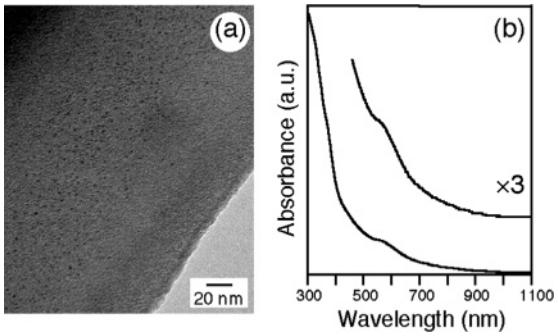

Figure 2. (a) TEM image and (b) UV−vis absorption spectrum of the as-prepared Au:SG clusters.

integrated spectral areas are conserved:

$$I(E) = I(w)/(\partial E/\partial w) \propto I(w) \times w^2 \quad (1)$$

where the $\partial E/\partial w$ term represents the Jacobian factor.

2.7. X-ray Photoelectron Spectroscopy (XPS). XPS measurement was performed using an electron spectrometer (ESCALAB 220iXL, Vacuum Generators) equipped in a chamber with the base pressure of ca. 2×10^{-8} Torr. The X-rays from the Mg Kα line at 1253.6 eV (15 kV, 20 mA) were used for excitation. The specimen was prepared by dropcasting the methanol dispersion of a sample onto a polished copper plate. Photoelectrons were collected in the constant analyzer energy mode with a pass energy of 20 eV. The binding energies were corrected by referencing the binding energies of Cu(3p) and Cu($2p_{3/2}$) arising from the substrate.

2.8. Fourier Transform Infrared Spectroscopy (FTIR). Infrared spectra were recorded on an FTIR spectrometer (FT/IR-4200, JASCO) with the resolution of 4 cm^{-1} in the transmission mode by accumulating 200 scans. The specimens were prepared by pressing KBr powder mixed with a powdered sample into a pellet.

3. Results and Discussion

3.1. Chemical Compositions. The ligation of glutathione in the form of the thiolate (GS) to the Au core was confirmed by the absence of the absorption band at $\nu(S-H) = 2526$ cm^{-1} in the FTIR spectrum of the as-prepared cluster sample (Figure S1). Figure 2 shows the TEM image and optical absorption spectrum of the as-prepared Au:SG clusters. The particles with the sizes of ∼1 nm are barely discernible in the image. The optical spectrum exhibits an onset at ∼1000 nm and a distinct shoulder at ∼580 nm. Both of the observations clearly illustrate that very small Au:SG clusters are efficiently formed under the conditions described in section 2.2. Since the core sizes of the resulting clusters are generally determined by relative rates between nucleation and growth, the formation of the small Au:SG clusters can be ascribed to retardation of the growth of the Au nuclei under the low-temperature conditions and by efficient passivation by GSH.

Figure 3 shows the results of the PAGE separation of the as-prepared Au:SG and Au:S(h-G) clusters. The as-prepared Au:SG clusters are clearly separated into several fractions, which we refer to as **1**−**9** in the order of the mobility. Note that fraction **1** having the highest mobility is visible to the eye only under the irradiation of a UV lamp. In contrast, the separation of the Au:S(h-G) clusters is less clear. The poorer separation for the Au:S(h-G) clusters is probably due to impurities associated with the h-GSH sample, which were detected by mass spectrometry (Figure S2). We collected five fractions, named as **1′**−**5′**, out of the gel, which are relatively isolated from the neighbors.

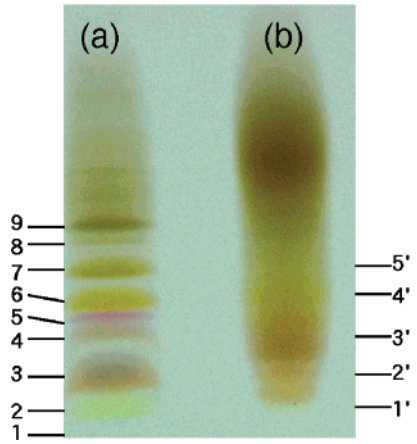

Figure 3. PAGE results for the (a) Au:SG and (b) Au:S(h-G) clusters.

One can anticipate that the Au:SG clusters are negatively charged in the sprayed solution since most of the carboxyl groups of the GS ligands tend to be dissociated; the acid dissociation constants of the two carboxyl groups of free GSH are 2.56 and 3.50.[69] As expected, the negative-ion ESI mass spectra of **1**−**9** are comprised of a series of peaks associated with multiply charged anions formulated as $[Au_n(SG)_m - xH]^{x-}$, where *n*, *m*, and *x* represent the numbers of gold atoms, GS ligands, and dissociated protons, respectively (left panels of Figure 4).[71] The right panels represent the $Au_n(SG)_m$ spectra reproduced from the mass peaks having the largest intensities among a series of the multiply charged peaks. Note that the quality of the mass spectra shown in Figure 4 is remarkably improved as compared with those in our previous report;[57] (1) the side peaks of the main peaks, which are tentatively assigned to the Cl adducts,[72] are suppressed considerably by using the Au:SG clusters freshly prepared; (2) the resolution of the mass spectrometer is improved by employing the reflectron; (3) the mass scale is calibrated more precisely by referencing the mass peaks of the $Na_nI_{n+1}^-$ clusters from a NaI aqueous solution recorded under the same experimental setup. Thanks to the improvements of the spectral quality, the mass spectra of **1**−**9** can be assigned unambiguously to the compounds listed in Table 1, whose mass spectra calculated from the isotopic abundance are shown by the colored peaks in Figure 4. Fractions **2**−**7** contain single species, whereas **1**, **8**, and **9** are composed of a few Au clusters of neighbored sizes. It is important to note that the assignments listed in Table 1 are different from those in our previous study.[57] For example, compound **6**, which has been assigned to $Au_{28}(SG)_{16}$ (10 415 Da) in our previous paper,[57] is reassigned to $Au_{25}(SG)_{18}$ (10 437 Da). The new assignments are further confirmed by comparing with the results of the Au:

(71) The mass peaks associated with the parent clusters were not discernible in the ion-spray mass spectrum of **6** recorded by using an LCMS-2010A (Shimadzu). The negative-ion mass spectrum was dominated by the fragment peaks assigned as $[Au(SG)_2\text{-}H]^{-1}$ (*m*/*z* 808) and $[Au_2(SG)_2\text{-}H]^{-1}$ (*m*/*z* 1005) (Figure S6). The remarkable difference in the mass spectra is probably due to that in the sampling region of the sprayed cone. The central region of the sprayed cone enriched by the heavy, multiply charged parent clusters with low volatility is efficiently sampled in our collinear configuration between the spray needle and the heated capillary (Figure 1b). In contrast, the periphery of the cone is mainly sampled in the orthogonal configuration between the needle and the sampling orifice of the LCMS-2010A apparatus (see, for example: Hiraoka, K.; Murata, K.; Kudaka, I. *Rapid Commun. Mass Spectrom.* **1993**, *7*, 363).

(72) Chlorine atoms originated from the starting material ($AuCl_4^-$) are probably left behind on the cluster surfaces, as in the case of the preparation of $Au_{55}(PPh_3)_{12}Cl_6$ by reduction of Ph_3PAuCl (Schmid, G. *Inorg. Synth.* **1990**, *7*, 214).

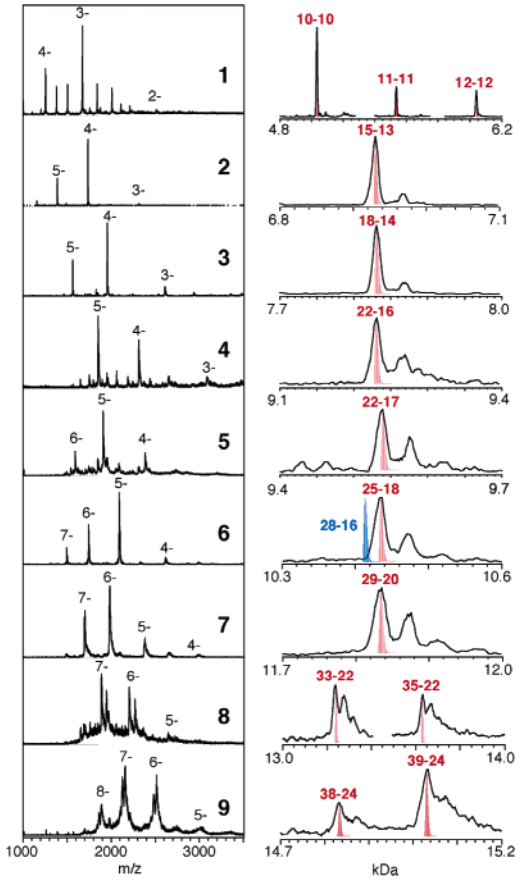

Figure 4. Low-resolution ESI mass spectra of the fractionated Au:SG clusters (left). The mass spectra reproduced from the most intense peaks in the high-resolution spectra (right). The calculated spectra for $Au_n(SG)_m$ are shown by the colored peaks with the corresponding $n-m$ values.

Table 1. Chemical Compositions and Yields of **1**−**9**

fraction	formula	yield (mol %)
1	$Au_{10}(SG)_{10}$, $Au_{11}(SG)_{11}$, $Au_{12}(SG)_{12}$	21[a]
2	$Au_{15}(SG)_{13}$	12
3	$Au_{18}(SG)_{14}$	23
4	$Au_{22}(SG)_{16}$	8
5	$Au_{22}(SG)_{17}$	7
6	$Au_{25}(SG)_{18}$	11
7	$Au_{29}(SG)_{20}$	9
8	$Au_{33}(SG)_{22}$, $Au_{35}(SG)_{22}$	3[a]
9	$Au_{38}(SG)_{24}$, $Au_{39}(SG)_{24}$	6[a]

[a] Calculated from the molecular weights of the most dominant species in the fractions.

S(h-G) clusters. Figure 5 shows the low-resolution ESI mass spectra of **1′**−**5′**. Although the purity of each fraction is not so high, it is evident that the Au:S(h-G) clusters of the same compositions as those in Table 1 are indeed formed in the sample. The chemical identities of **1**−**9** are not disrupted by the workup for the mass analysis since the mass analysis (Figure S3) shows that the as-prepared cluster sample is a mixture of the compounds listed in Table 1. The experimental procedure described above has been established through our repeated experiences and reproducibly provides us the isolated compounds listed in Table 1. Also listed in Table 1 are the typical molar yields of **1**−**9**, calculated from the measured weight (e.g., 2.8 mg of $Au_{18}(SG)_{14}$ from a single gel) and molecular weight of each compound; the contamination from the gel is estimated

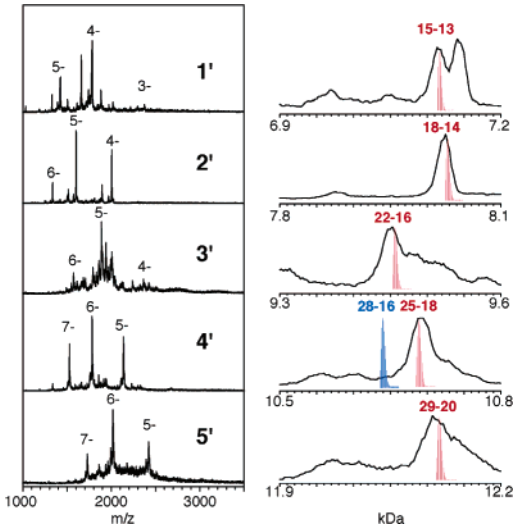

Figure 5. Low-resolution ESI mass spectra of the fractionated Au:S(h-G) clusters.

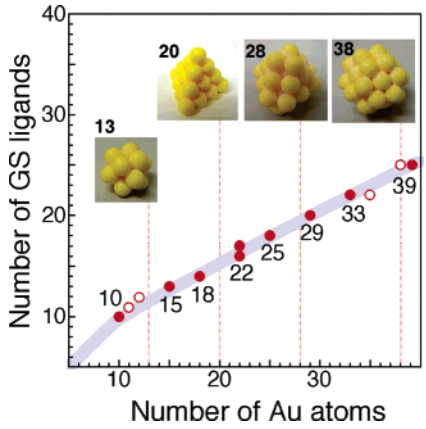

Figure 6. A plot of the chemical compositions of **1**−**9** against the number of Au atoms and GS ligands. The closed and open dots represent the most dominant and minor species contained in the fractions, respectively. The numbers depicted near the closed circles are the core sizes of the most dominant species. The models shown in the inset indicate the structures of highly symmetrical fcc crystals.

to be less than 5 wt % from the NMR spectra and blank experiments so that it is ignored in the calculations. Compounds **1**−**3** and **6** are relatively abundant as compared with the others. This trend is qualitatively reproduced although the quantitative yields are somewhat dependent on the original cluster samples. All of the compounds are found to be stable against unimolecular decomposition either in aqueous solution or in a powder form as long as they are stocked in a refrigerator (<2 °C).

3.2. Stability and Origin of Preferential Formation. The PAGE separation and mass analysis demonstrated that a series of the Au:SG clusters with well-defined composition is preferentially formed. This finding shows that compounds **1**−**9** are relatively stable as compared with other sized clusters. Let us first examine a possibility that the high stabilities of **1**−**9** are originated exclusively from those of the Au cores as in the case of thiolate-protected Au NCs. In Figure 6 are plotted the numbers of the Au atoms and GS ligands of **1**−**9**. The most remarkable feature of the plot is that the core sizes of **1**−**9** scarcely match neither the "magic numbers" of free Au_n clusters associated with closing of the electronic shells (n = 8, 18, 20,

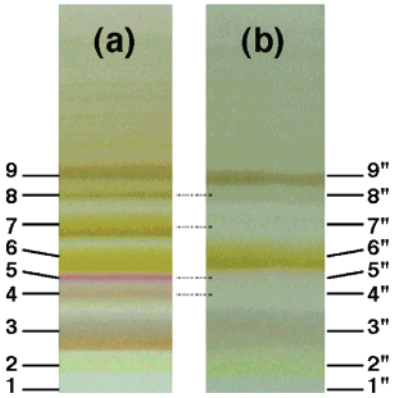

Figure 7. PAGE results of the Au:SG clusters (a) prepared freshly and (b) stored in aqueous solution for 2 weeks under ambient conditions in the dark.

34, ...)[73−77] nor those of geometrical shells (n = 13, 20, 28, 38, ...).[44,45,47,78,79] This finding is in sharp contrast with the successful preparation of a tetrahedral Au_{20} cluster weakly coordinated by phosphine ligands[78] and an Au_8 cluster within an internal cavity of a dendrimer.[80] Thus, the core sizes of **1**−**9** are not determined solely by intrinsic stabilities of the Au cores, but are affected strongly by the thiolate ligation. As a possible mechanism of the thiolate-induced stabilization, we have suggested in our previous paper[57] that partial charge transfer at the Au−S interfaces[44,45] can stabilize certain sized cores due to the closing of the electronic shells. However, the isolation of $Au_{22}(SG)_{16}$ and $Au_{22}(SG)_{17}$, for example, does not allow us to explain the stabilities of the Au:SG clusters by a simple electron counting scheme where constant charge transfer is assumed for each Au−S bond. Another plausible role of the thiolate ligation on the preferential formation of **1**−**9** is selective stabilization of the certain sized Au clusters by completion of the ligand shells. The consecutive core growth is kinetically hindered at every stage where the core is completely surrounded by the thiolate ligand shell during a head-on competition between the growth and passivation of the Au cores. One notices a trend from Figure 6 that the Au core sizes increase by 3−4 atoms in every increment of a GS ligand, suggesting the Au clusters fitted in size to the volumes of the cavities made by the ligand shells are preferentially stabilized. Namely, the Au:SG clusters isolated here possibly correspond to trapped intermediates of the growing clusters, whose surfaces are fully passivated.

The stabilities of **1**−**9** against unimolecular decomposition have been studied in order to gain further insight into their inherent stabilities. The aqueous solution of the as-prepared Au:SG clusters was stored for 2 weeks under ambient conditions. The PAGE separation of the sample thus treated gives fractions **1**″−**9**″ having comparable mobilities with those of **1**−**9**, respectively (Figure 7). The gel image shown in Figure 7 clearly illustrates that the bands associated with **4**, **5**, **7**, and **8** become faint, indicating that they are relatively unstable against decomposition as compared with the others. The optical spectra of **4**″, **5**″, **7**″, and **8**″ show that the chemical identities of **4**, **5**, **7**, and **8** are lost during the storage (Figure S4); ESI mass analysis of the stock solutions of isolated compounds **4**, **5**, **7**, and **8** revealed that $Au_{18}(SG)_{14}$, $Au_{20}(SG)_{14}$, $Au_{25}(SG)_{18}$, and $Au_{28}(SG)_{18}$ were formed as the decay products. In contrast, the mass spectra and optical spectra of **1**″−**3**″, **6**″, and **9**″ are essentially identical with those of **1**−**3**, **6**, and **9**, respectively (Figure S4). The results indicate that compounds **1**−**3**, **6**, and **9** are much more stable than the others against the unimolecular decomposition. The enhanced stability of **1**−**3**, **6**, and **9** may arise from the formation of a stable protecting shell through hydrogen-bonded networks among the GS ligands. Large populations of **1**−**3**, **6**, and **9** (Table 1) are explained in terms of their thermodynamic stabilities. Therefore, it is concluded that compounds **1**−**9** are populated preferentially, reflecting their kinetic stabilities against further nucleation, and that their relative populations are determined by the thermodynamic stabilities.

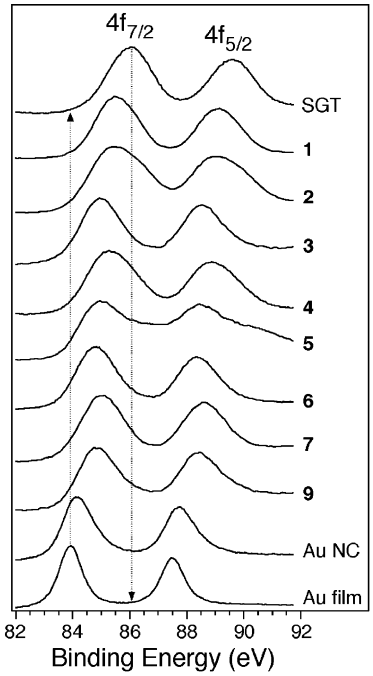

Figure 8. The Au(4f) XPS spectra of the Au:SG clusters (**1**−**7**, and **9**). The vertical dotted lines represent the Au($4f_{7/2}$) binding energies of sodium Au(I) thiomalate (SGT) and Au(0) film. The spectrum of the Au:SG NCs with an average size of 1.8 nm (σ = 0.6 nm) is shown for comparison.

3.3. Evolution of Geometric and Electronic Structures. Figure 8 shows the Au 4f core-level photoemission spectra of the Au:SG clusters (**1**−**7** and **9**), sodium Au(I) thiomalate (SGT), Au:SG NCs (1.8 ± 0.3 nm, Figure S5), and the Au(0) film measured at room temperature. The Au(4f) peak positions of the Au:SG clusters are located between those of the Au(I) thiolate complex and Au(0) film. The Au(4f) peak widths of the Au:SG clusters are appreciably broader than those of the Au NCs and Au(0) film. These features are qualitatively interpreted on the basis of the recent XPS studies on the thiolate-protected Au NCs with diameters in the range of 1.6−5.2 nm.[81−83] Tanaka and co-workers have found from the detailed

(73) Katakuse, I.; Ichihara, T.; Fujita, Y.; Matsuo, T.; Sakurai, T.; Matsuda, H. *Int. J. Mass Spectrom. Ion Processes* **1985**, *67*, 229.
(74) Kim, H. S.; Wood, T. D.; Marshall, A. G.; Lee, J. Y. *Chem. Phys. Lett.* **1994**, *224*, 589.
(75) Taylor, K. J.; Pettiette-Hall, C. L.; Cheshnovsky, O.; Smalley, R. E. *J. Chem. Phys.* **1992**, *96*, 3319.
(76) de Heer, W. A. *Rev. Mod. Phys.* **1993**, *65*, 611.
(77) Li, J.; Li, X.; Zhai, H.-J.; Wang, L.-S. *Science* **2003**, *299*, 864.
(78) Zhang, H.-F.; Stender, M.; Zhang, R.; Wang, C.; Li, J.; Wang, L.-S. *J. Phys. Chem. B* **2004**, *108*, 12259.
(79) Nobusada, K. *J. Phys. Chem. B* **2004**, *108*, 11904.
(80) Zheng, J.; Petty, J. T.; Dickson, R. M. *J. Am. Chem. Soc.* **2003**, *125*, 7780.
(81) (a) Zhang, P.; Sham, T. K. *Phys. Rev. Lett.* **2003**, *90*, 245502. (b) Moriarty, P. *Phys. Rev. Lett.* **2004**, *92*, 109601. (c) Zhang, P.; Sham, T. K. *Phys. Rev. Lett.* **2004**, *92*, 109602.

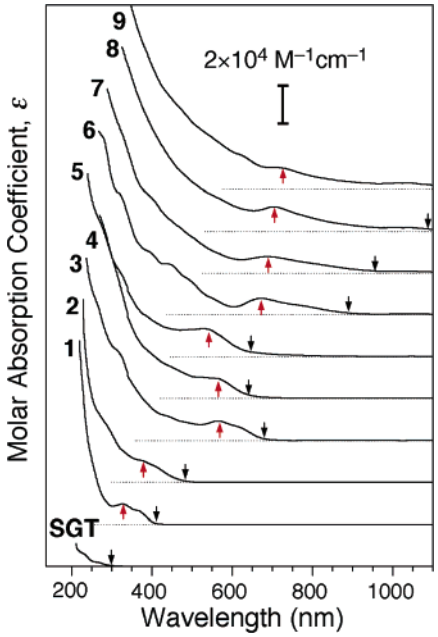

Figure 9. Optical absorption spectra of aqueous solutions of **1**−**9** and sodium Au(I) thiomalate (SGT) at ambient temperature.

peak shape analysis that the Au($4f_{7/2}$) peaks are deconvoluted into two components originating from the inner and surface atoms of the gold NCs.[82,83] The Au($4f_{7/2}$) peak positions for the inner Au were found to be monotonically shifted from 84.0 to 84.3 eV with the reduction of the core size. This trend is explained in terms of "final-state effect", where the photocreated hole left behind the NC lowers the kinetic energy of the outgoing photoelectron through the Coulomb attractive force. In contrast, the Au($4f_{7/2}$) peak positions of the surface Au components have been located higher in energy (84.3−84.7 eV) than the corresponding inner components; the electron donation occurs from the surface Au atoms to the thiolates ("initial-state effect"). Since the Au($4f_{7/2}$) binding energies of the Au:SG clusters are ∼85 eV and most of the Au atoms are located on the core surface for such small clusters, it is reasonable to conclude that the chemical shifts observed here are mostly due to the initial-state effect.[81] Namely, electron donation occurs from the Au core to the GS ligands in the Au:SG clusters substantially, but to a smaller extent than in the Au(I)−thiolate complexes, being consistent with theoretical prediction.[44,45] The broadening of the Au(4f) peaks for the Au:SG clusters possibly reflects the inhomogeneity in the degree of electron donation depending on the binding sites of the thiolates.

Figure 9 summarizes the optical absorption spectra of the aqueous solutions of **1**−**9** and SGT[9] at ambient temperature. Spectral profiles of **1**−**9** are in sharp contrast with those of thiolate-protected Au NCs (>2 nm), which exhibit the surface plasmon band at ∼520 nm on otherwise smooth exponential-like profiles.[25,27,28] Clear absorption onsets in the range of 400−1000 nm appear, which are indicated by downward arrows in Figure 9. The onsets are followed by humps, which tend to be blue shifted with a decrease in the core size, as indicated by upward arrows. The molar extinction coefficients for the lowest-energy bands of **1**−**9** are calculated on the basis of the molecular weights determined by mass spectrometry and are summarized in Table 2. These features demonstrate that the electronic structures of compounds **1**−**9** are well quantized and are better viewed as nonmetallic molecular assemblies rather than metallic particles protected by thiolates. Although we must await theoretical studies to fully assign the optical spectra shown in Figure 9, the spectra can be qualitatively interpreted with the help of the recent density functional studies on the photoabsorption spectra of small Au clusters protected by methanethiolates, such as Au(SCH_3), $Au_3(SCH_3)$, $Au_{13}(SCH_3)_8^{3+}$, and $Au_{18}(SCH_3)_8$.[79,84] For example, the optimized structure of $Au_{13}(SCH_3)_8^{3+}$ within O_h symmetry is composed of a cuboctahedral Au_{13} core whose (111) facets are passivated by eight CH_3S ligands.[79] The absorption spectrum of $Au_{13}(SCH_3)_8^{3+}$ exhibits two sharp peaks at 532 and 395 nm and shoulder structures at 224−268 nm. The former two peaks have been assigned to the transitions from the high-lying occupied Au 6s orbitals to the low-lying unoccupied Au 6s/6p orbitals. The latter bands at higher energy region have been assigned to the transitions from the Au−S bonding or Au 5d orbitals to the unoccupied Au 6s/6p orbitals. These optical transitions correspond to the "intraband" and "interband" transitions of the bulk gold, respectively, so that we conveniently borrow these terminologies to describe the optical transitions of the Au:SG clusters. Although the peak positions are dependent on the chemical compositions of the thiolated clusters, the systematic theoretical studies have revealed a general trend of the optical spectra; the peaks associated with the intraband and interband transitions appear in the energy regions below and above ∼4 eV, respectively.[84] By applying this criterion, we assign the peaks denoted by the upward arrows and broad bands in the UV region of **1**−**9** to the transitions corresponding to the Au 6sp intraband and interband transitions of the bulk gold, respectively.

Let us consider whether compound **1**, the smallest species obtained, is better categorized as a Au(I)−thiolate complex or as a thiolated Au cluster. The chemical composition of [Au]:[GS] = 1:1 suggests that compound **1** has the structure similar to the Au(I)−thiolate complexes. Indeed, our preliminary DFT study on the model compound, $Au_{10}(SCH_3)_{10}$, predicts a ring structure with −Au−S(CH_3)− repeated bondings as a stable species. However, compound **1** has several features that distinguish it from the Au(I)−thiolate complex as listed below. (i) The lowest absorption band calculated for the cyclic Au_{10}-

Table 2. Optical Properties of **1**−**9**

fraction	ε ($M^{-1}cm^{-1}$)/ first peak (nm)[a]	emission maximum (eV)	Φ_{PL}[b]	core mass (kDa)[c]	SW sample[d]/core mass (kDa)[e]
1	1.1×10^4/330	1.5/3.0	$1 \times 10^{-4}/8 \times 10^{-6}$	1.970	
2	1.2×10^4/370	1.5/2.9	$2 \times 10^{-4}/1 \times 10^{-5}$	2.955	
3	1.1×10^4/570	1.5	4×10^{-3}	3.546	**1**/4
4	1.1×10^4/560	1.6	4×10^{-3}	4.344	**1′**
5	1.5×10^4/540	1.7	2×10^{-3}	4.344	
6	8.8×10^3/670	1.5	1×10^{-3}	4.925	**2**/6
7	8.5×10^3/690	1.4	3×10^{-3}	5.713	**2′**/∼7
8	1.3×10^4/710	1.4	2×10^{-3}	6.501	
9	1.1×10^4/730	1.4	2×10^{-3}	7.683	**3**/8

[a] Shown by upward arrows in Figure 9. [b] PL quantum yield. [c] Calculated from the formula of the most dominant species in the fraction. [d] Notation given in ref 59. [e] Determined by MALDI-MS (ref 59).

(82) Tanaka, A.; Takeda, Y.; Imamura, M.; Sato, S. *Phys. Rev. B* **2003**, *68*, 195415.
(83) Tanaka, A.; Takeda, Y.; Nagasawa, T.; Takahashi, K. *Solid State Commun.* **2003**, *126*, 191.
(84) Nobusada, K.; Shiratori, K. Private Communication.

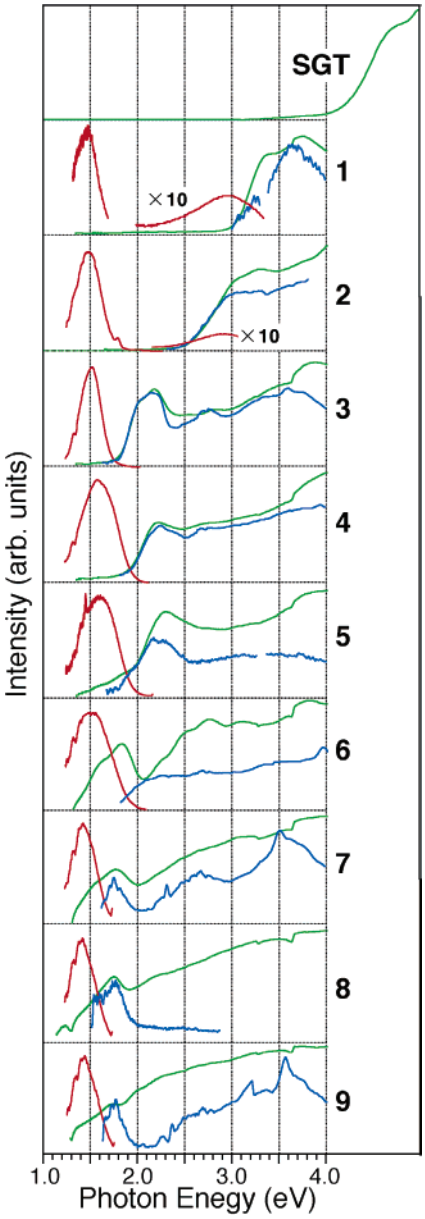

Figure 10. Optical absorption (green), photoemission (red), and photoexcitation (blue) spectra of aqueous solutions of **1**−**9** at ambient temperature.

$(SCH_3)_{10}$ polymer appears at the region of <300 nm, as in the case of SGT (Figure 9). In contrast, compound **1** exhibits an absorption band in the range of 300−400 nm assignable to the Au 6sp intraband transition (Figure 9). (ii) The XPS spectra (Figure 8) show that the Au atoms in **1** are less cationic than that of SGT. (iii) Compound **1** in aqueous solution is emissive upon the photoexcitation of the Au 6sp intraband transition, whereas SGT is not[9] (see Figure 10). We take this emissive property as the evidence for Au−Au bonding in **1** on the basis of an empirical rule that the Au−Au interaction is necessary to observe photoluminescence.[6−11] These marked differences indicate that even the smallest species of $Au_{10}(SG)_{10}$ obtained here is not categorized as a Au(I)−thiolate complex but is classified as the thiolated Au cluster. This inference inevitably means that all the Au atoms are located on the core surface and are bonded to the GS ligands. We speculate a tetrahedral-like motif for the Au_{10} core of $Au_{10}(SG)_{10}$, where all of the Au atoms are on the core surface.

Close inspection of Figure 9 shows that the absorption bands associated with the Au 6sp intraband transitions are not shifted monotonically with increase in the core size, but are red shifted abruptly on going from **1** to **3** and from **5** to **6**. Such irregular behavior in the optical spectra implies discontinuous sequence in the core growth. The abrupt red shift of the spectral onsets (Figure 9) and reduction of the [GS]:[Au] ratio between **1** and **3** (Figure 6) may be due to the involvement of Au atoms free from thiolate bonding in the core structures. Formation of another Au layer may start between **5** and **6**. It is worth noting here that the $Au_{22}(SG)_{16}$ and $Au_{22}(SG)_{17}$ clusters exhibit appreciably different optical spectra, although their cores consist of the same number of Au atoms. Since the absorption in the visible region is associated with the intraband transitions, the difference in the spectral profile suggests the thiolate ligation appreciably modifies the frontier orbitals through charge transfer and/or core deformation as theoretically predicted by Garzón and co-workers.[46−48]

Now we are in a position to compare the results presented here with those previously reported by Schaaff and Whetten (SW)[59] and our group.[57] The comparison of the optical spectra and molecular weights (Table 2) establishes that the fractions denoted as **1**, **1′**, **2**, **2′**, and **3** by SW[59] correspond to our compounds **3**, **4**, **6**, **7**, and **9**, respectively. Namely, one of the dominant cluster compounds, which has been assigned as $Au_{28}(SG)_{16}$ by SW,[59] should again be reassigned to $Au_{25}(SG)_{18}$. The missing of compounds **1** and **2** in the previous experiments[57,59] is probably because they were scarcely visible to the eye and/or because such small species were not formed efficiently in their experimental conditions (room temperature and $[AuCl_4^-]$:[GSH] = 1:2). Compounds **5** and **8** are relatively unstable against decomposition, as described in section 3.2, so that they might be degradated during the sample handling in the previous studies.[57]

The molecular-like electronic structures of **1**−**9** manifest themselves in the photoluminescence (PL) behavior. We show in Figure 10 the photoemission, photoexcitation, and photoabsorption spectra of **1**−**9**. Table 1 summarizes the emission energies and PL quantum yields, Φ_{PL}, of **1**−**9**. The Φ_{PL} values of **1**−**9** are remarkably larger than that of the bulk gold ($\Phi_{PL} = 10^{-10}$),[85] showing the enhanced contribution of radiative process in the decay of the photoexcited states for these small systems. The excitation spectra, except for that of **6**, trace well the profiles of the corresponding absorption spectra (Figure 10), indicating that the sp intraband excitations are responsible for the photoemission. From this observation, we tentatively assign that the emission bands at ∼3 eV for **1** and **2** and those at 1.4−1.7 eV for **3**−**5** and **7**−**9** originate from radiative intraband transitions within the sp bands across the HOMO−LUMO gap. The low-energy emission band at ∼1.5 eV for **1** and **2** probably originates from the sp excited states of different spin multiplicities populated via intersystem crossing. In contrast, the lowest-energy peak at ∼1.8 eV observed in the absorption spectra of **6** is missing in the excitation spectra, as pointed out previously by Link et al.[52] The origin of this irregular PL behavior of $Au_{25}(SG)_{18}$ is not clear at the present time. The results reported here (Table 2) and previously[50−57] have revealed that the thiolated Au clusters tend to emit photons in the range of 1.0−1.7 eV with Φ_{PL} on the order of 10^{-3}−10^{-5}. In contrast, small Au

(85) Mooradian, A. *Phys. Rev. Lett.* **1969**, *22*, 185.

clusters (Au_5, Au_8, Au_{13}, Au_{23}, Au_{31}) entrapped within dendrimers are highly fluorescent, with Φ_{PL} as large as 10^{-1}; the emission energies are fitted by a simple relation, $E_{Fermi}(\text{cluster size})^{-1/3}$, predicted by the jellium model.[86] These contrasted PL properties clearly demonstrate significant effects of the thiolate passivation on the electronic structures and photophysical properties of the small Au clusters.

4. Conclusion

We report herein synthesis and characterization of a series of Au_n clusters ($n = 10-39$) protected by glutathione ligands by using PAGE separation and ESI mass spectrometry. The spectroscopic measurements of these fractionated clusters revealed that they are molecular in nature and that their optical and photophysical properties are heavily dependent on the core sizes and the number of the thiolates. The spectral data clearly show the structural evolution of the thiolated Au clusters which supply the missing link between the Au(I)−thiolate complexes and thiolate-protected Au NCs. The experimental approach reported here is versatile and will be applicable to any systems composed of inorganic (metal, semiconductor) cluster cores and thiolate−ligand shells bearing net charge(s) on the surface (e.g., carboxyl and sulfonic groups). One of the important contributions of the present work is that the reproducible isolation and easy handling of the cluster compounds provide researchers a novel opportunity to study their fundamental properties by use of various experimental tools. We hope that the experimental data on the structures and properties of the cluster compounds thus accumulated will provide a useful guideline for the development of new organometallic artificial molecules with collaboration from theoretical investigations.

Acknowledgment. We thank Prof. K. Kimura (University of Hyogo) for providing the Au:SG samples at the initial stage of the research. Profs. H. Sakurai and K. Tanaka (IMS) are acknowledged for measuring NMR spectra and allowing us to use the LCMS-2010A apparatus, respectively. Prof. K. Takehara (Kyushu University) is appreciated for providing information on the Au:SG SAMs. The sample of sodium Au(I) thiomalate was provided by Shionogi Co. Ltd. The present work was financially supported by Grant-in-Aids for Scientific Research (Nos. 769 and 90262104) and the "Nanotechnology Support Project" from MEXT, Japan, the "2002th-year Joint Research Project" of Sokendai (Soken/K02-1), and Sumitomo Foundation.

Supporting Information Available: FTIR spectrum of the as-prepared Au:SG clusters (Figure S1), ESI mass spectra of GTR and h-GTR (Figure S2), ESI mass spectrum of the as-prepared Au:SG clusters (Figure S3), optical spectra of **1″**−**9″** (Figure S4), TEM image of the Au:SG NCs (Figure S5), and mass spectrum of **6** recorded by an LCMS-2010A apparatus (Figure S6, PDF). This material is available free of charge via the Internet at http://pubs.acs.org.

JA042218H

(86) Zheng, J.; Zhang, C.; Dickson, R. M. *Phys. Rev. Lett.* **2004**, *93*, 077402.